Journal of Sound and Vibration 348 (2015) 41–56

Contents lists available at ScienceDirect

Journal of Sound and Vibration

journal homepage: www.elsevier.com/locate/jsvi

Variable friction device for structural control based on duo-servo vehicle brake: Modeling and experimental validation

Liang Cao [a,*], Austin Downey [a], Simon Laflamme [a,b], Douglas Taylor [c], James Ricles [d]

[a] Department of Civil, Construction, and Environmental Engineering, Iowa State University, Ames, IA 50011, USA
[b] Department of Electrical and Computer Engineering, Iowa State University, Ames, IA 50011, USA
[c] Taylor Devices, North Tonawanda, NY 14120, USA
[d] Department of Civil and Environmental Engineering, Lehigh University, Bethlehem, PA 18015, USA

ARTICLE INFO

Article history:
Received 30 September 2014
Received in revised form
20 January 2015
Accepted 6 March 2015
Handling Editor: D.J. Wagg
Available online 29 March 2015

ABSTRACT

Supplemental damping can be used as a cost-effective method to reduce structural vibrations. In particular, passive systems are now widely accepted and have numerous applications in the field. However, they are typically tuned to specific excitations and their performances are bandwidth-limited. A solution is to use semi-active devices, which have shown to be capable of substantially enhanced mitigation performance. The authors have recently proposed a new type of semi-active device, which consists of a variable friction mechanism based on a vehicle duo-servo drum brake, a mechanically robust and reliable technology. The theoretical performance of the proposed device has been previously demonstrated via numerical simulations. In this paper, we further the understanding of the device, termed Modified Friction Device (MFD) by fabricating a small scale prototype and characterizing its dynamic behavior. While the dynamics of friction is well understood for automotive braking technology, we investigate for the first time the dynamic behavior of this friction mechanism at low displacements and velocities, in both forward and backward directions, under various hydraulic pressures. A modified 3-stage dynamic model is introduced. A LuGre friction model is used to characterize the friction zone (Stage 1), and two pure stiffness regions to characterize the dynamics of the MFD once the rotation is reversed and the braking shoes are sticking to the drum (Stage 2) and the rapid build up of forces once the shoes are held by the anchor pin (Stage 3). The proposed model is identified experimentally by subjecting the prototype to harmonic excitations. It is found that the proposed model can be used to characterize the dynamics of the MFD, and that the largest fitting error arises at low velocity under low pressure input. The model is then verified by subjecting the MFD to two different earthquake excitations under different pressure inputs. The model is capable of tracking the device's response, despite a lower fitting performance under low pressure and small force output, as it was found in the harmonic tests due to the possible nonlinearity in Stage 2 of the model.

* Corresponding author.
E-mail address: liangcao@iastate.edu (L. Cao).

http://dx.doi.org/10.1016/j.jsv.2015.03.011
0022-460X/

1. Introduction

Modern construction techniques and materials enable the construction of lighter and more flexible structures, thereby increasing wind-induced vibrations, as an example, which may lead to discomfort and frequent inoperability. Recent extreme events (e.g., earthquakes, hurricanes, tornadoes, storm surges) have demonstrated the utmost vulnerability of buildings and transportation infrastructures. A solution to increase structural performance vis-a-vis service and extreme loads is a motion-based design (MBD) approach. The strategy with MBD is to appropriately size structural stiffness and supplemental damping for a given mass system to restrict motion to a prescribed performance [1].

In particular, supplemental damping has been shown to be cost-effective in mitigating structural vibrations. Passive damping systems are now widely accepted in the field of structural control given their low maintenance, passive operability, and mechanical robustness [2]. Among these systems, passive friction devices combine the advantage of being (1) capable of high energy dissipation independent of velocity; (2) inexpensive; (3) easy to install; and (4) relatively low maintenance [2,3]. However, their strong nonlinear behavior, degradation of sliding interface, possibility of cold weld, and reliability on a restoring force are strong disadvantages, most likely responsible for their lack of popularity with respect to viscous dampers.

Numerous passive friction devices for structural damping have been proposed since the late 1970s. Pall et al. [4] and Pall and Marsh [5] developed the Pall friction damper, a frictional braces that dissipates energy via a slip bolted joint. Other types of friction connections have been studied in Refs. [6–8]. More recently, Morgen and Kurama [9], Lin et al. [10] proposed friction dampers for dissipating energy at a beam-column joint. Panchal and Jangid [11] proposed a variable friction pendulum system for base-isolation. Mirtaheri et al. [12] proposed a cylindrical friction damper.

Semi-active friction systems have been proposed to significantly enhance energy dissipation using low power. The additional controllability is provided by an actuation system that varies the normal force applied on the friction mechanism. Examples of actuators include hydraulic [13], pneumatic [14,15], electro-magnetic [16,17], electro-mechanical [18,19] and piezoelectric [20–23].Large semi-active friction capacities reported in the literature include a 2 kN piezoelectric friction device from Lu et al. [21], a 3 kN electromagnetic friction damper from Dai et al. [24], and 20 kN capacity electromagnetic and electromechanical devices from Agrawal et al. [25] and Narasimhan et al. [18], respectively. The authors have presented a novel variable friction device termed the Modified Friction Device (MFD) [26], which has a theoretical damping capacity of 200 kN, which is larger than that of the large semi-active friction devices reported above. The dynamics of the MFD is based on a duo-servo automobile brake, using hydraulic or pneumatic actuation, and leverages the self-energizing feature of the brake to amplify the actuation force. While the device showed great promise because of its large damping force capability and mechanically reliable technology, work presented on the MFD was purely theoretical.

In this paper, we further understand the MFD by characterizing its dynamic behavior. While friction dynamics of automotive braking systems has been studied for several decades, none of the studies found in the literature examined the dynamics of vehicle braking technology utilized in both forward and backward directions, as it would be utilized to mitigate structural vibrations. Furthermore, most models focused on large displacements and high velocities. Here, the dynamic behavior of the MFD is investigated at low displacements and velocities, in both forward and backward directions, under various pressures (force inputs). A dynamic model is introduced, which consists of three stages of dynamics. A LuGre friction model is used to characterize the friction zone (Stage 1), and two pure stiffness regions to characterize the dynamics of the MFD once the rotation is reversed and the braking shoes are sticking to the drum (Stage 2) and the rapid build up of forces once the shoes are held by the anchor pin (Stage 3). A small-scale prototype is built by directly modifying an automobile brake due to its readily availability, and the proposed model is validated experimentally.

The paper is organized as follows. Section 2 provides the theoretical background on the MFD and discusses the fabrication of the prototype. Section 3 presents the proposed 3-stage dynamic model. Section 4 identifies the parameters of the dynamic model by subjecting the prototype to harmonic excitations at 0.05 Hz and 0.50 Hz, under various pressure inputs. Section 5 validates the model by subjecting the device to two different earthquake excitations. Section 6 concludes the paper.

2. Background

The MFD is designed to dissipate energy via friction developed by the contact of braking shoes onto a drum. Fig. 1 shows a schematic representation of the MFD showing the internal components (Fig. 1(a)) and the diagram of forces (Fig. 1(b)). This friction dynamics of the MFD is described in details in Ref. [26]. Briefly, the actuation force $W=pA$, where p is the actuation pressure and A the area of the actuator, acts on the braking shoes (the thick blue line in Fig. 1 shows the shoes' lining) to create normal forces N_i on shoes $i=1, 2$, which in turn generate friction forces f_i, with the total friction force $F=f_1+f_2$. Installed in a vertical configuration, the MFD is designed to sit on two short support legs that produce opposite forces F_{leg} to counteract the moment produced by the friction forces. Fig. 2 illustrates two possible configurations of the MFD installed within a bracing scheme. The first one is a chevron bracing configuration, and the second one is a toggle bracing configuration. The toggle bracing configuration has the advantage of largely amplifying the movement of the floor drift transmitted to the damping device, which would allow the MFD to attain the Coulomb friction faster, but is more expensive to install [27]. For both configurations, the floor drift $\delta=x/H$ is transformed into rotational displacement θ of the MFD using

$$y=\theta r \tag{1}$$

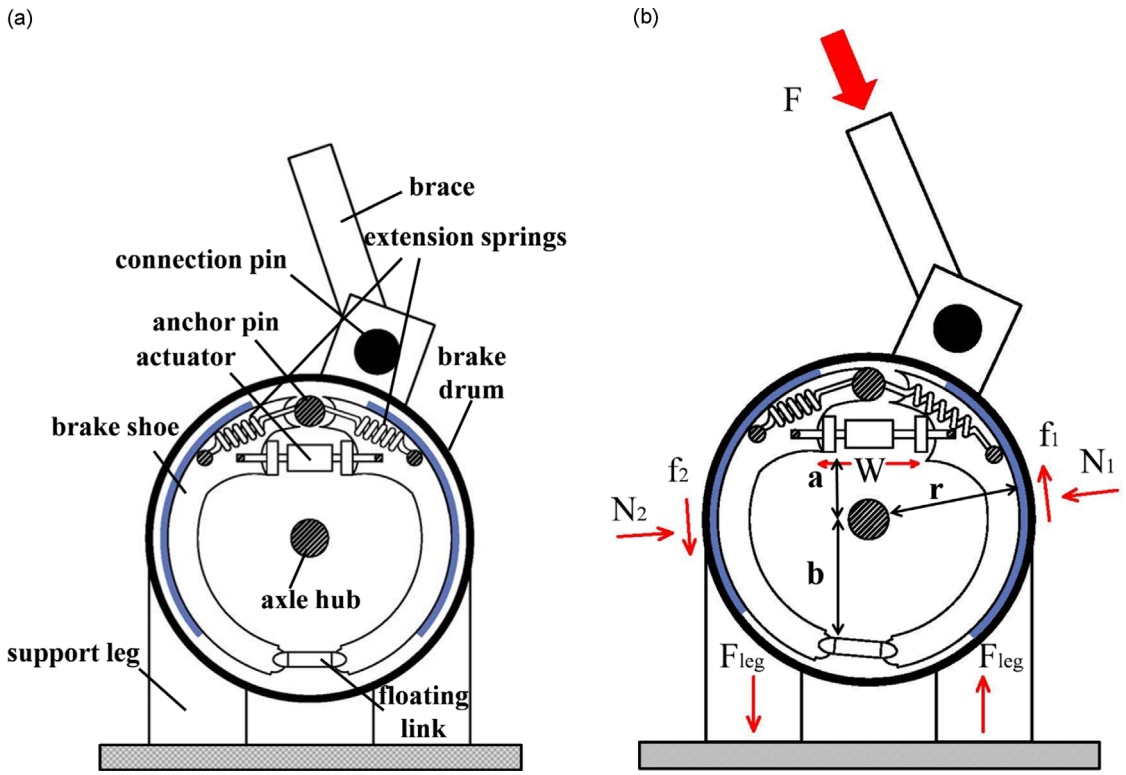

Fig. 1. Schematic representation of the MFD: (a) internal components and (b) diagram of forces.

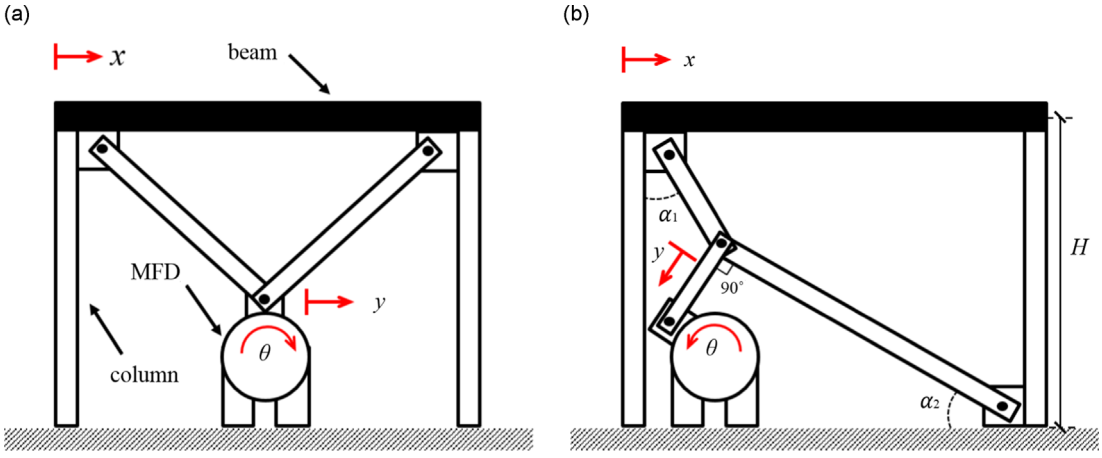

Fig. 2. MFD placement within bracing systems: (a) chevron configuration and (b) toggle configuration. Red arrows illustrate displacement. (For interpretation of the references to color in this figure caption, the reader is referred to the web version of this article.)

where x is the translational displacement of the floor, H is the height of the floor, y is the tangential displacement of the drum, and r is the radius of the drum.

For the chevron configuration (Fig. 2(a)), $y=x$, giving

$$\theta = \frac{\delta H}{r} \tag{2}$$

Ref. [28] provides the analytical solution relating δ to y for the toggle configuration shown in Fig. 2(b). For small angles, it can be shown that [29]

$$y = \frac{\sin \alpha_1}{\cos(\alpha_1 + \alpha_2)} x \tag{3}$$

or

$$\theta = \frac{\sin\alpha_1}{\cos(\alpha_1+\alpha_2)}\frac{\delta H}{r} \tag{4}$$

Eqs. (2) and (4) provide an approximate linear relation between θ and δ, which can be used in performance-based design to size the damper [1]. For example, the approximate stroke of the MFD in a chevron configuration under a story drift $\delta = 0.02$ rad provoked by a maximum considered earthquake level would be $\theta = 0.56$ rad for a floor height $H = 14$ ft and

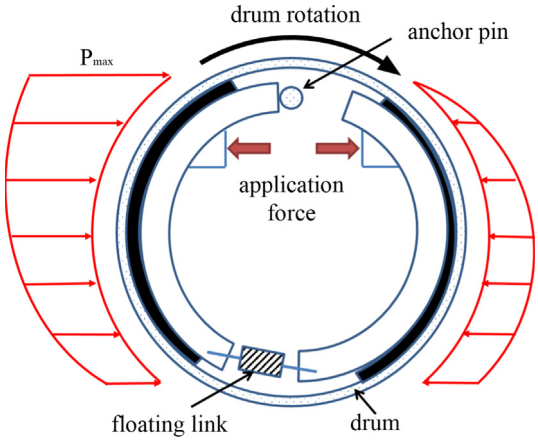

Fig. 3. Self-energizing effect distribution for duo-servo drum brake.

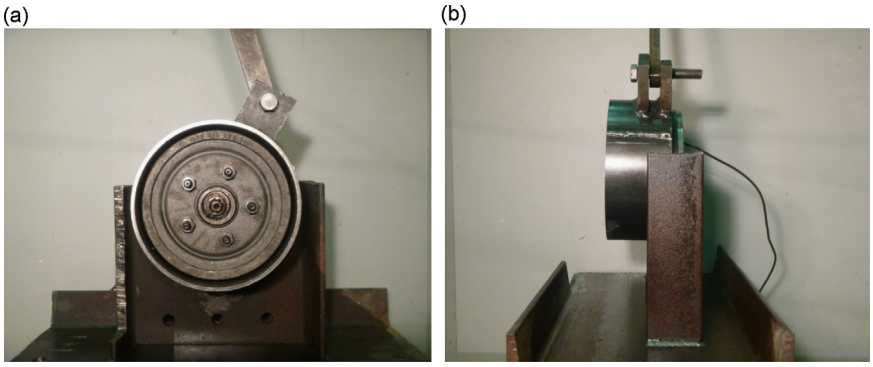

Fig. 4. Prototype of the MFD: (a) front view and (b) side view.

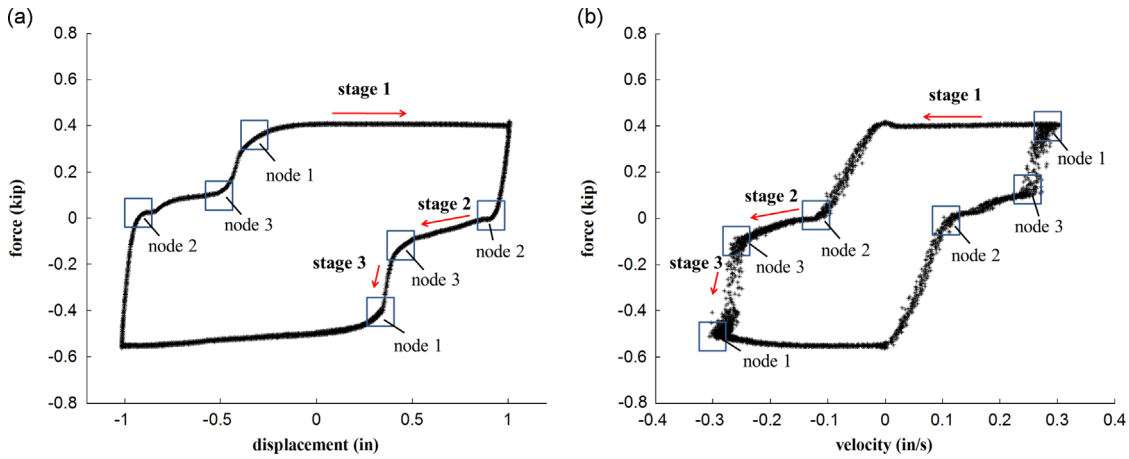

Fig. 5. Dynamic response of the MFD under hydraulic pressure of 1200 psi: (a) force–displacement plot (0.05 Hz) and (b) force–velocity plot (0.05 Hz).

drum radius $r=6$ in. This is equivalent to a circumferential displacement of 3.36 in, which is substantially beyond the full friction development length of the prototype under study. The performance of the device can be optimized under a performance-based design approach [1] by altering the geometry of the damper and the bracing system.

Table 1
Parameters of the MFD dynamic model.

Parameter	Stage	Pressure dependence
$F_{c,\mathrm{fwd}}$	1	$F_{c,\mathrm{fwd}}=C_{c,\mathrm{fwd}}p$
$F_{c,\mathrm{bwd}}$	1	$F_{b,\mathrm{fwd}}=C_{b,\mathrm{fwd}}p$
$F_{s,\mathrm{fwd}}$	1	$F_{s,\mathrm{fwd}}=C_{s,\mathrm{fwd}}p$
$F_{s,\mathrm{bwd}}$	1	$F_{b,\mathrm{fwd}}=C_{b,\mathrm{fwd}}p$
σ_0	1	$\sigma_0=\alpha_{\sigma_0}p+\sigma_0\vert_{p=0}$
σ_1	1	None
σ_2	1	None
k_2	2	None
k_3	3	None
d_2	2	None
d_3	3	None
γ_1	1–3	None
γ_2	1–3	None

Note: p is the input pressure, and $C_{c,\mathrm{fwd}}$, $C_{c,\mathrm{bwd}}$, $C_{s,\mathrm{fwd}}$, $C_{s,\mathrm{bwd}}$, and α_{σ_0} are constants.

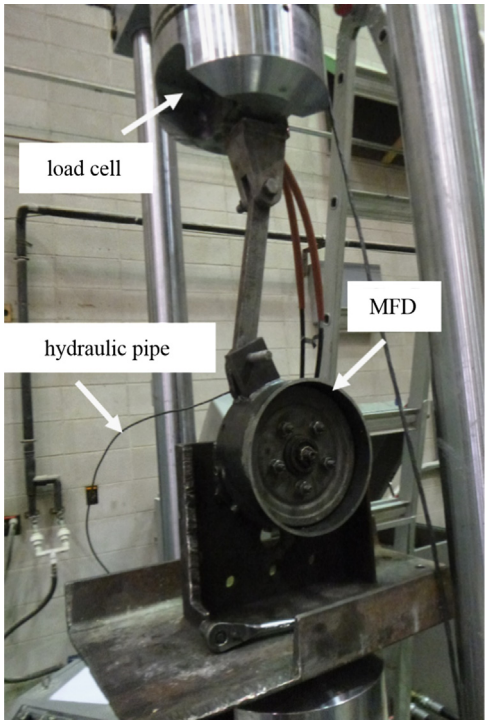

Fig. 6. Experimental setup.

Table 2
Pressure dependent model parameters: results from 0.05 Hz.

Parameter	0 psi		500 psi		800 psi		1200 psi		1500 psi	
	Exp.	Model	Exp.	Model	Exp.	Model	Exp.	Model	Exp.	Model
$F_{c,\mathrm{fwd}}$ (kip)	0.002	0.000	0.142	0.170	0.239	0.273	0.403	0.409	0.530	0.512
$F_{c,\mathrm{bwd}}$ (kip)	−0.004	0.000	−0.181	−0.229	−0.295	−0.366	−0.549	−0.548	−0.710	−0.686
$F_{s,\mathrm{fwd}}$ (kip)	0.005	0.000	0.152	0.175	0.251	0.280	0.417	0.420	0.549	0.525
$F_{s,\mathrm{bwd}}$ (kip)	−0.006	0.000	−0.185	−0.236	−0.305	−0.374	−0.563	−0.560	−0.727	−0.701
σ_0 (kip · in^{-1})	N/A	3.029	4.054	4.029	4.754	4.629	5.054	5.429	6.254	6.029

Table 3
Pressure dependent model parameters: results from 0.5 Hz.

Parameter	0 psi		500 psi		800 psi		1200 psi		1500 psi	
	Exp.	Model	Exp.	Model	Exp.	Model	Exp.	Model	Exp.	Model
$F_{c,\mathrm{fwd}}$ (kip)	0.002	0.000	0.143	0.170	0.260	0.273	0.412	0.409	0.536	0.512
$F_{c,\mathrm{bwd}}$ (kip)	−0.003	0.000	−0.183	−0.229	−0.340	−0.366	−0.587	−0.548	−0.710	−0.686
$F_{s,\mathrm{fwd}}$ (kip)	0.005	0.000	0.155	0.175	0.269	0.280	0.417	0.420	0.538	0.525
$F_{s,\mathrm{bwd}}$ (kip)	−0.006	0.000	−0.188	−0.236	−0.341	−0.374	−0.595	−0.560	−0.730	−0.701
σ_0 (kip · in^{-1})	N/A	3.029	4.082	4.029	4.702	4.629	5.282	5.429	6.222	6.029

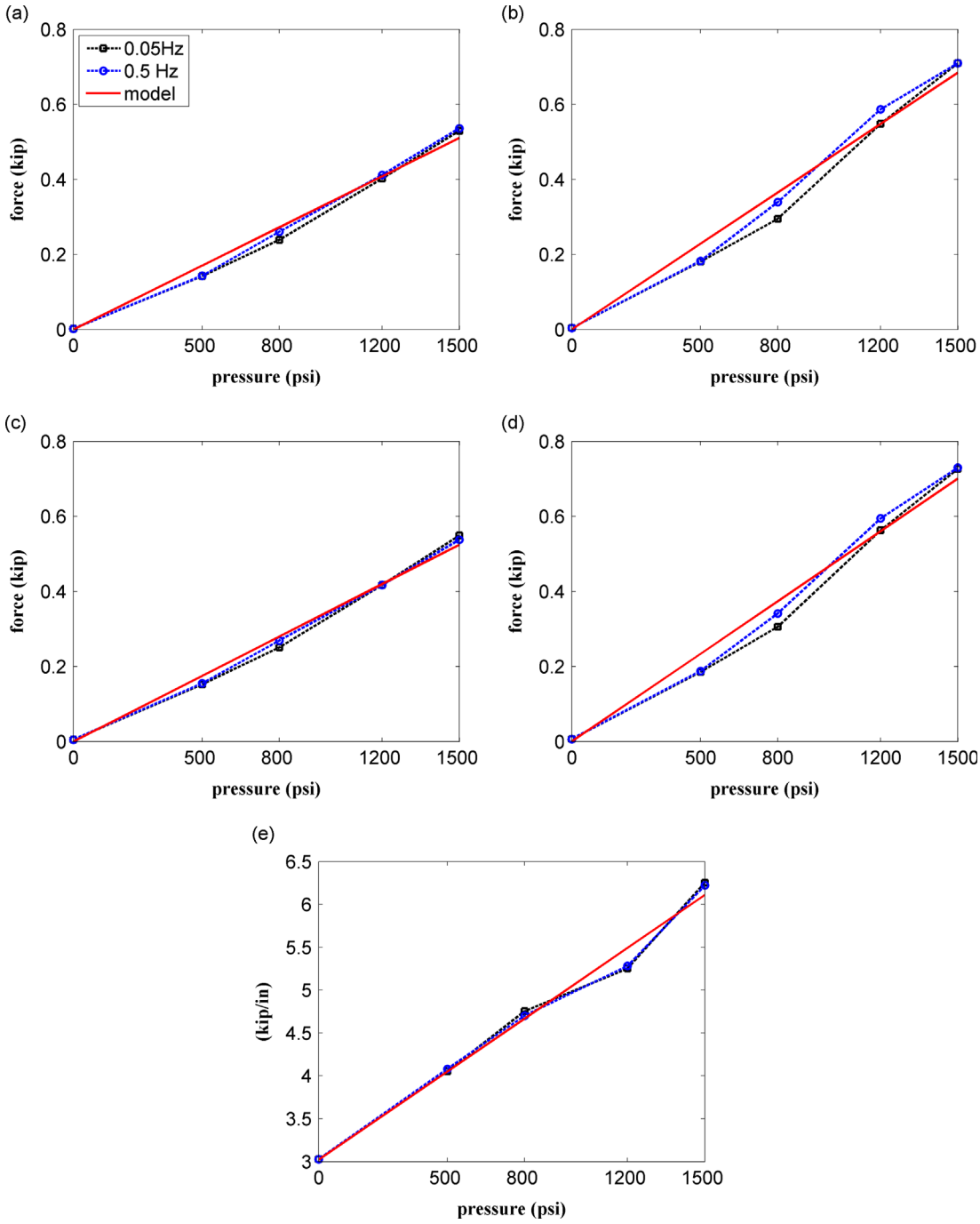

Fig. 7. Comparison of model values and test values: (a) $F_{c,\mathrm{fwd}}$; (b) $F_{c,\mathrm{bwd}}$; (c) $F_{s,\mathrm{fwd}}$; (d) $F_{s,\mathrm{bwd}}$; (e) σ_0.

The duo-servo drum brake illustrated in Fig. 1 is slightly different that the one presented in Ref. [26]. The fabricated prototype presented in this paper is an altered version of a vehicle brake, as it will be described later. A duo-servo vehicle brake exhibits a gap between the anchor pin and the shoes, which is a necessary feature to provide continuous

Table 4
Pressure independent parameters in model.

Parameter	Units	Value
α_{σ_0}	in^{-3}	2.000
$\sigma_0\|_{p=0}$	$\text{kip}\cdot\text{in}^{-1}$	3.029
σ_1	$\text{psi}\cdot\text{s}\cdot\text{in}^{-1}$	1.000
σ_2	$\text{psi}\cdot\text{s}\cdot\text{in}^{-1}$	1.000
k_2	$\text{kip}\cdot\text{in}^{-1}$	0.231
k_3	$\text{kip}\cdot\text{in}^{-1}$	3.000
d_2	in	0.500
d_3	in	0.200
γ_1	in	1.000
γ_2	in	0.100
$C_{c,\text{fwd}}$	$\text{kip}\cdot\text{in}^{-2}$	0.341
$C_{c,\text{bwd}}$	$\text{kip}\cdot\text{in}^{-2}$	0.457
$C_{s,\text{fwd}}$	$\text{kip}\cdot\text{in}^{-2}$	0.350
$C_{s,\text{bwd}}$	$\text{kip}\cdot\text{in}^{-2}$	0.467

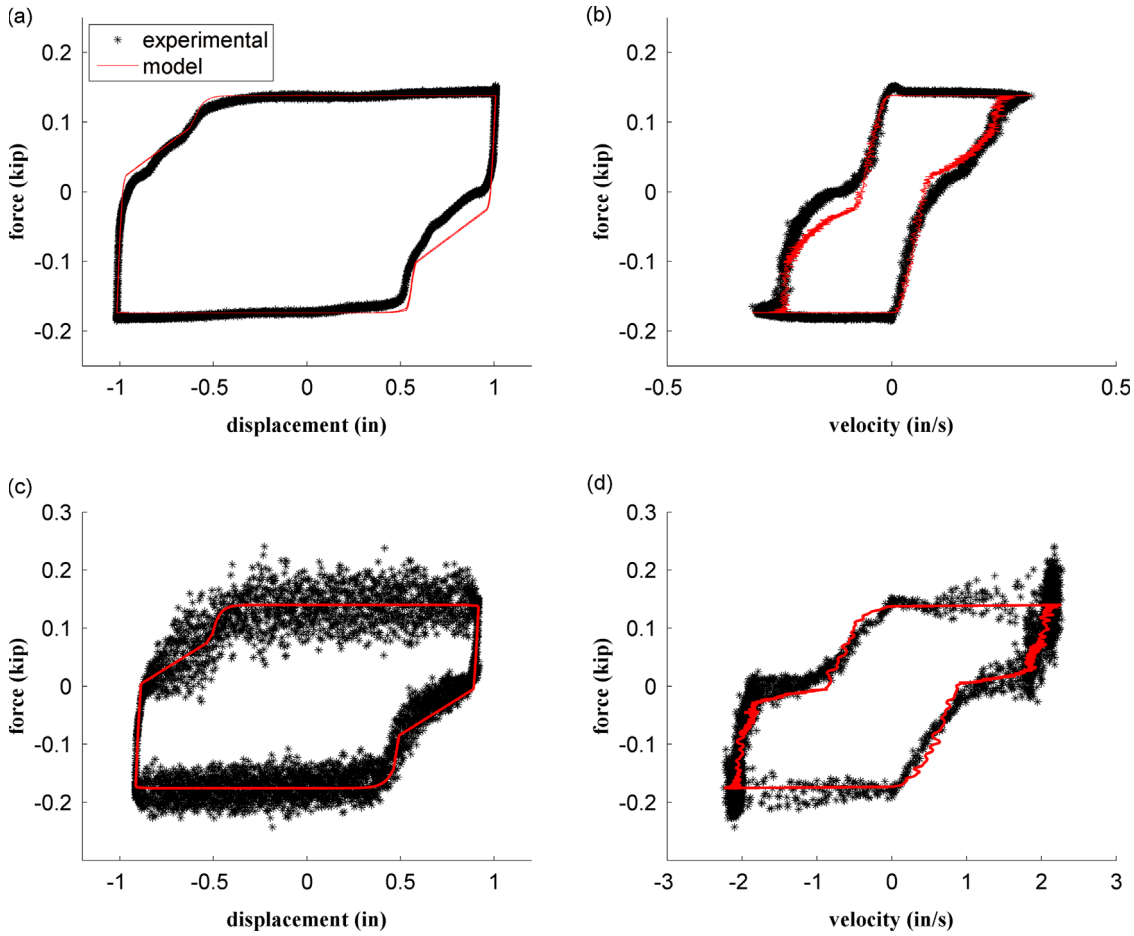

Fig. 8. Harmonic test at 500 psi: (a) force–displacement (0.05 Hz); (b) force–velocity (0.05 Hz); (c) force–displacement (0.5 Hz); (d) force–velocity (0.5 Hz).

self-energizing throughout both shoes. The self-energizing mechanism amplifies the actuation force W by a factor C for a total friction force $F=CW$. It is a result of a static moment generated from the position and geometry of the shoes with respect to the drum. As the drum rotates and the braking mechanism is applied, the drum gradually drags the shoes along the circumference which produces an increasing friction force, as shown in Fig. 3. P_{max} is the maximum pressure caused by self-energizing effect. The amplification factor C is a constant that can be calculated using the following equation [30]:

$$C=\frac{\mu(a+b)}{a\sqrt{1+\mu^2}-\mu r}\left[1+\left(\frac{a+r}{r}\frac{\sqrt{1+\mu^2}}{1-\mu}\right)\right]-\frac{a+b}{r}\frac{\mu}{1-\mu} \tag{5}$$

where μ is the friction coefficient of the lining material, r is the radius of the drum, a is the distance between floating link and center of the drum, and b is the distance between actuator and center of the drum.

2.1. Prototype

A prototype of the MFD has been fabricated by slightly altering an automotive car brake due to the readily availability of the mechanical components. The drum brake has been rotated under constant hydraulic pressure during several hours in both directions to wear the lining surface, in order to produce friction forces of similar magnitude in both forward and backward directions. The drum was mounted on a structural steel C-section to allow a vertical axial loading configuration. In this particular setup, torsion is negligible, and the moment generated by the friction force is counteracted by the moment generated in the fixture's legs, as shown in Fig. 1(a). A similar configuration could be used to install the MFD in a structural system, for instance within a diagonal bracing element. The force W is generated by a hand-operated hydraulic actuator. Note that in a typical installation, a pneumatic actuator could be used. The dynamic interaction actuator-brake is out-of-the-scope of this paper. A picture of the built prototype is shown in Fig. 4.

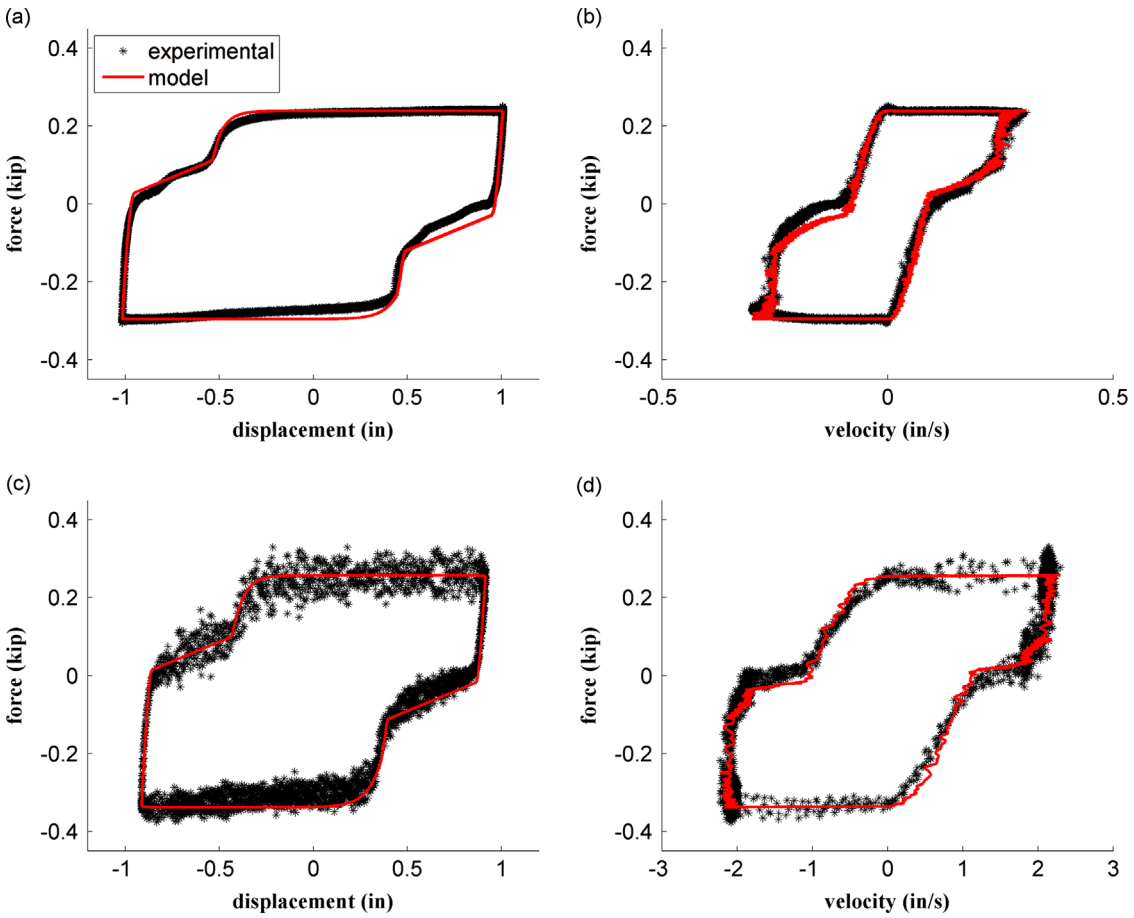

Fig. 9. Harmonic test at 800 psi: (a) force–displacement (0.05 Hz); (b) force–velocity (0.05 Hz); (c) force–displacement (0.5 Hz); (d) force–velocity (0.5 Hz).

3. Dynamic model

The operational performance of the MFD over a full forward and backward motion is characterized by friction dynamics over most of the rotation. The presence of a gap between the anchor pin and braking shoes, as discussed above and shown in Fig. 1, is responsible for a discontinuity in the friction dynamics when the rotation is reversed. Upon rotation, the leading shoe sticks to the drum until it hits the anchor pin. During this process, the MFD behaves like a stiffness element. Once the leading shoe hits the anchor pin, there is a rapid build up in the resisting force, until the friction dynamics is recovered. A typical response of the MFD over an harmonic excitation period is shown in Fig. 5 to illustrate these dynamic stages (taken at ± 1 in, 0.05 Hz, and 1200 psi constant pressure input). The proposed dynamic model to characterize the behavior of the MFD is as follows:

- Stage 1 (Node 1 ⟶Node 2): The system is in a typical dynamic friction mode. The friction force F_1 is characterized using a LuGre friction model. This stage occurs until rotation is reversed and the frictional force is lost.
- Stage 2 (Node 2 ⟶Node 3): Braking shoes are sticking to the drum. The linear force F_2 is characterized as being proportional to a stiffness element k_2. This stage occurs over a drum displacement d_2.
- Stage 3 (Node 3 ⟶Node 1): One braking shoe is anchored at the anchor pin, and there is a rapid force build up. The force build up is coming from the shock when the braking shoes hit the anchor pin which generate the stiffness. The force F_3 is characterized as being proportional to a stiffness element k_3. This stage occurs over a drum displacement d_3.

A smooth transition region between these stages is introduced. It consists of a C^∞ function of the following type [31]:

$$m(x) = \frac{1}{1+e^{-(\gamma_1(x-x_0))/\gamma_2}} \tag{6}$$

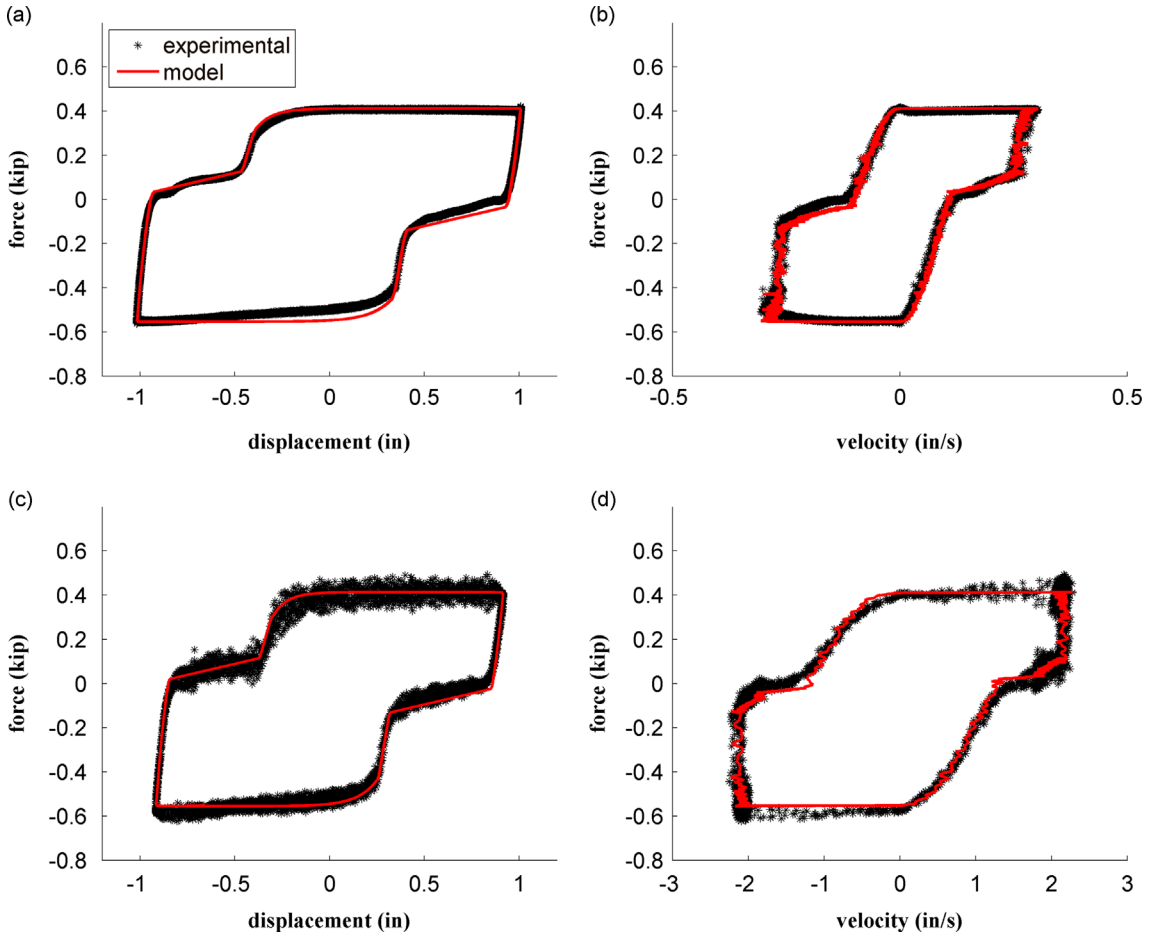

Fig. 10. Harmonic test at 1200 psi: (a) force–displacement (0.05 Hz); (b) force–velocity (0.05 Hz); (c) force–displacement (0.5 Hz); (d) force–velocity (0.5 Hz).

where x_0 is the reference displacement of the new stage, and γ_1, γ_2 are constants. Consider the transition from stage i to stage j. The total force F is given by

$$F = (1 - m(x))F_i + m(x)F_j \tag{7}$$

The next subsection describes the LuGre model used to characterize the friction dynamics, and the subsequent subsection introduces the remaining model parameters.

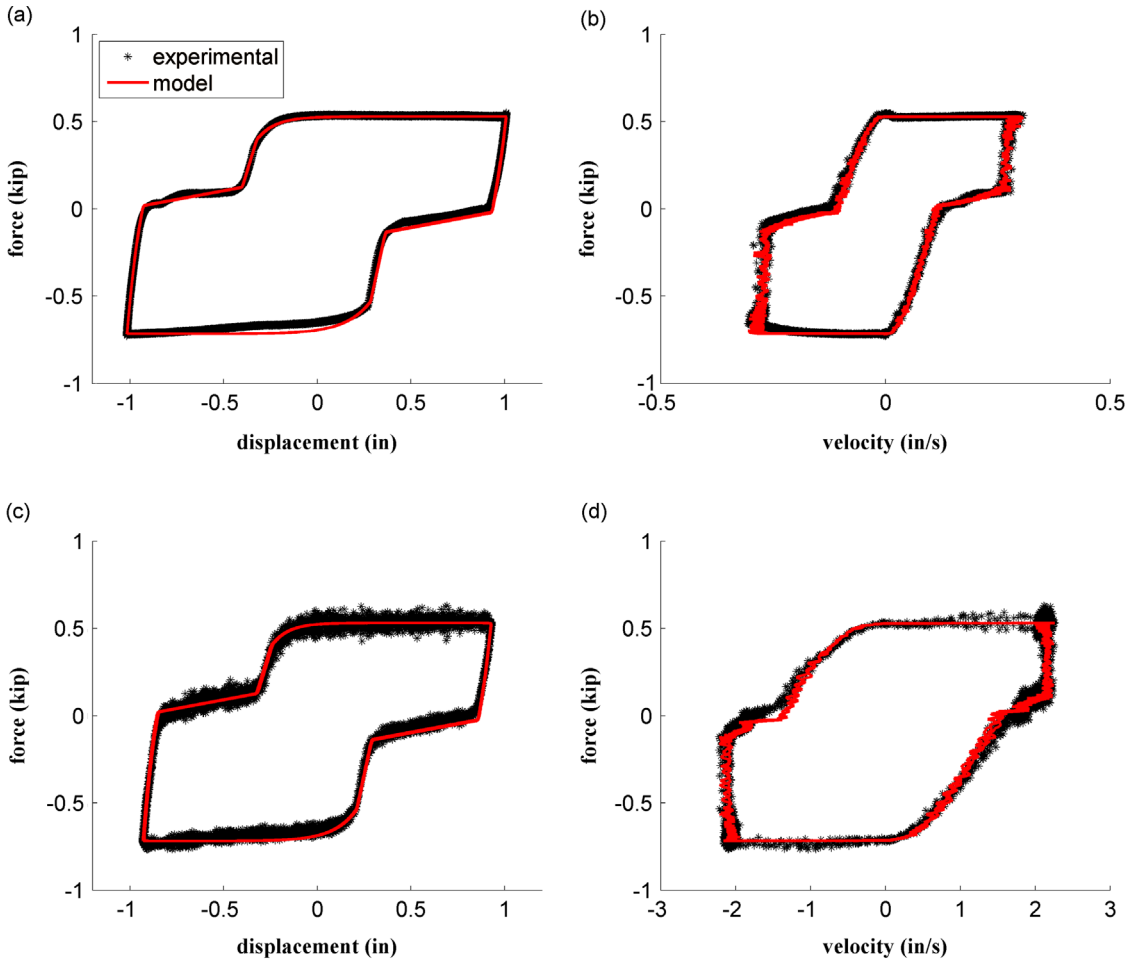

Fig. 11. Harmonic test at 1500 psi: (a) force–displacement (0.05 Hz); (b) force–velocity (0.05 Hz); (c) force–displacement (0.5 Hz); (d) force–velocity (0.5 Hz).

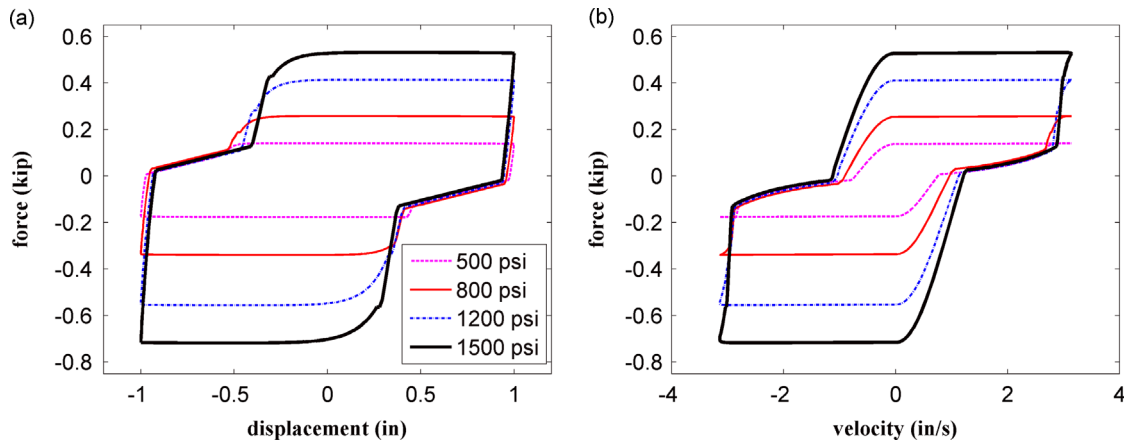

Fig. 12. (a) Force–displacement and (b) force–velocity loops for a harmonic excitation of 1 in at 0.50 Hz.

3.1. LuGre model

The LuGre model is selected to characterize the friction dynamics due to its capability to accurately simulate the Stribeck effect and rate dependance of the friction phenomenon [32]. The LuGre model has been applied to a wide range of systems, including other semi-active devices such as the magnetorheological damper [33].

Using this model, the resisting force during stage 1 F_1 is a friction force written as follows:

$$F_1 = \sigma_0 z + \sigma_1 \dot{z} + \sigma_2 \dot{x}$$
$$\dot{z} = \dot{x} - \sigma_0 \frac{|\dot{x}|}{g(\dot{x})} z \tag{8}$$

where σ_0 represents the aggregate bristle stiffness, σ_1 – microdamping, σ_2 – viscous friction, z – an evolutionary variable, x and $\dot{x}$ – the displacement and velocity, respectively, and $g(\dot{x})$ – a function that describes the Stribeck effect:

$$g(\dot{x}) = F_c + (F_s - F_c) e^{-(\dot{x}/\dot{x}_s)^2} \tag{9}$$

In Eq. (9) $\dot{x}_s$ is a constant modeling the Stribeck velocity, F_s the static frictional force, and F_c the kinetic frictional force.

Due to the surface irregularities, friction coefficients are different between forward and backward rotations, as evidenced in Fig. 5, where the maximum and minimum forces have difference values. F_s and F_c are allowed to take two different values whether the brake rotates forwards ($F_{s,\mathrm{fwd}}$ and $F_{c,\mathrm{fwd}}$) or backwards ($F_{s,\mathrm{bwd}}$ and $F_{c,\mathrm{bwd}}$).

3.2. Model parameters

The parameters used in the characterization of the MFD are listed in Table 1. Note that friction forces ($F_{s,\mathrm{fwd}}$, $F_{c,\mathrm{fwd}}$, $F_{s,\mathrm{bwd}}$ and $F_{c,\mathrm{bwd}}$) and the aggregate bristle stiffness σ_0 are dependent on the input pressure. The linear function governing their behavior is also shown in Table 1. No parameters in the model are taken as frequency-dependent.

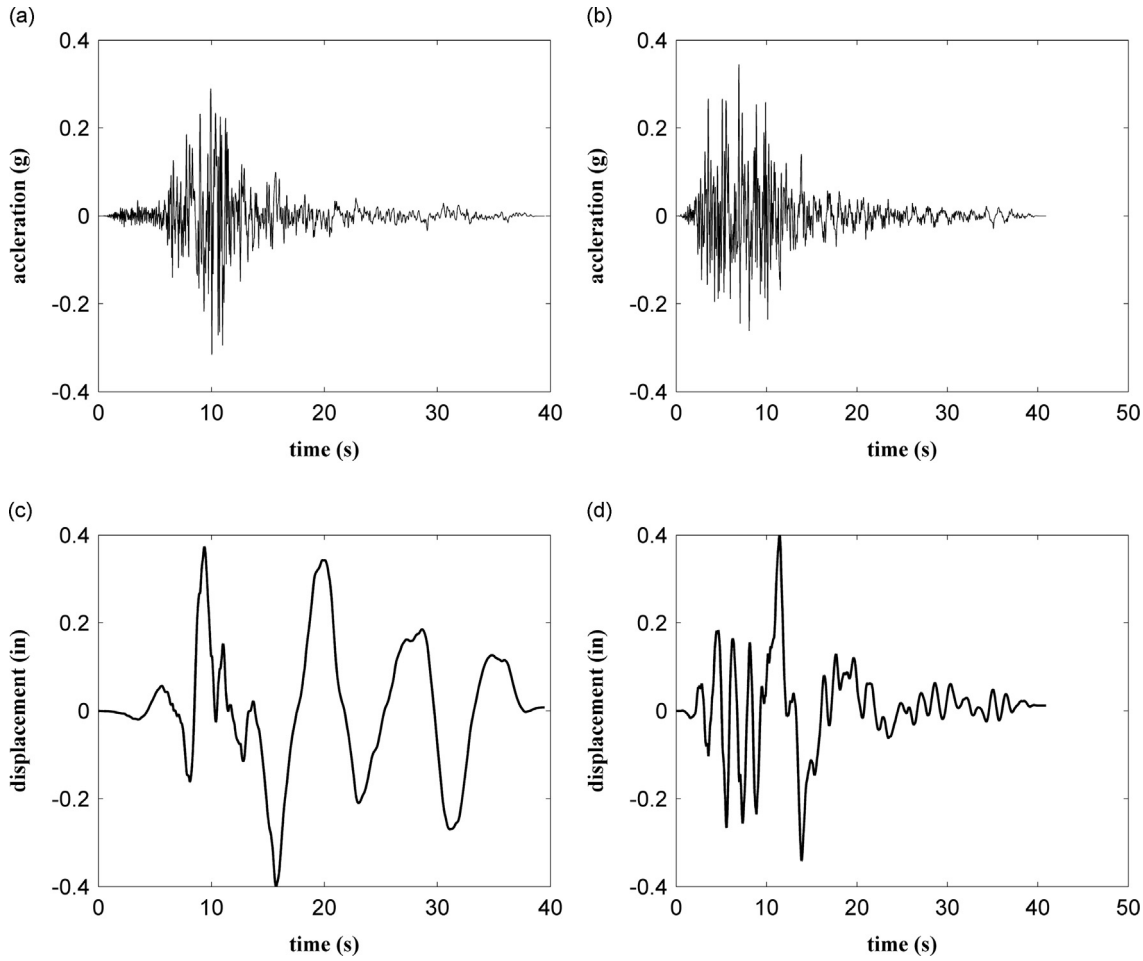

Fig. 13. Earthquake input excitations: (a) unscaled ground acceleration (Imperial Valley earthquake); (b) unscaled ground acceleration (Kobe earthquake); (c) scaled ground displacement (Imperial Valley earthquake); (d) scaled ground displacement (Kobe earthquake).

4. Identification of model parameters

4.1. Methodology

The identification of the model parameters was conducted by subjecting the MFD to harmonic excitations of 1 in amplitude at low frequency (0.05 Hz) and higher frequency (0.50 Hz). Five different pressures (force inputs) were tested: 0, 500, 800, 1200, and 1500 psi, where 1500 psi corresponds approximately to the actuator's maximum capacity (100 percent force), for a total of 10 tests. Tests were displacement-controlled, induced by an MTS 810 material testing system. Force and displacement data were recorded by the MTS data acquisition system at a 100 Hz sampling rate.The experimentally measured motion signals were used as input for the dynamic model. The experimental setup is shown in as shown in Fig. 6. Each test was ran over 10 cycles. The characterization of the parameters is based the average value of all cycles. The model characterized in this section will later be validated under a wider range of displacements and velocities by subjecting the device to earthquake excitations.

4.2. Experimental results

The model parameters for the proposed three-stage dynamic model were identified by minimizing the fitting error between experimental data and the dynamic model. The parameters are identified by minimizing the performance function J, which is taken as the error between the estimated friction force $\hat{F}_k$ from the model and the experimental friction force F for each test k:

$$J = \|\hat{F}_k - F_k\|_2 \tag{10}$$

where $\|\cdot\|_2$ is the 2-norm. This minimization is conducted in MATLAB by using the command `fminsearch` and using different arbitrary (and physically realistic) initial conditions. The parameters defining the pressure-dependence are obtained by a linear fit of the values obtained at different pressures.

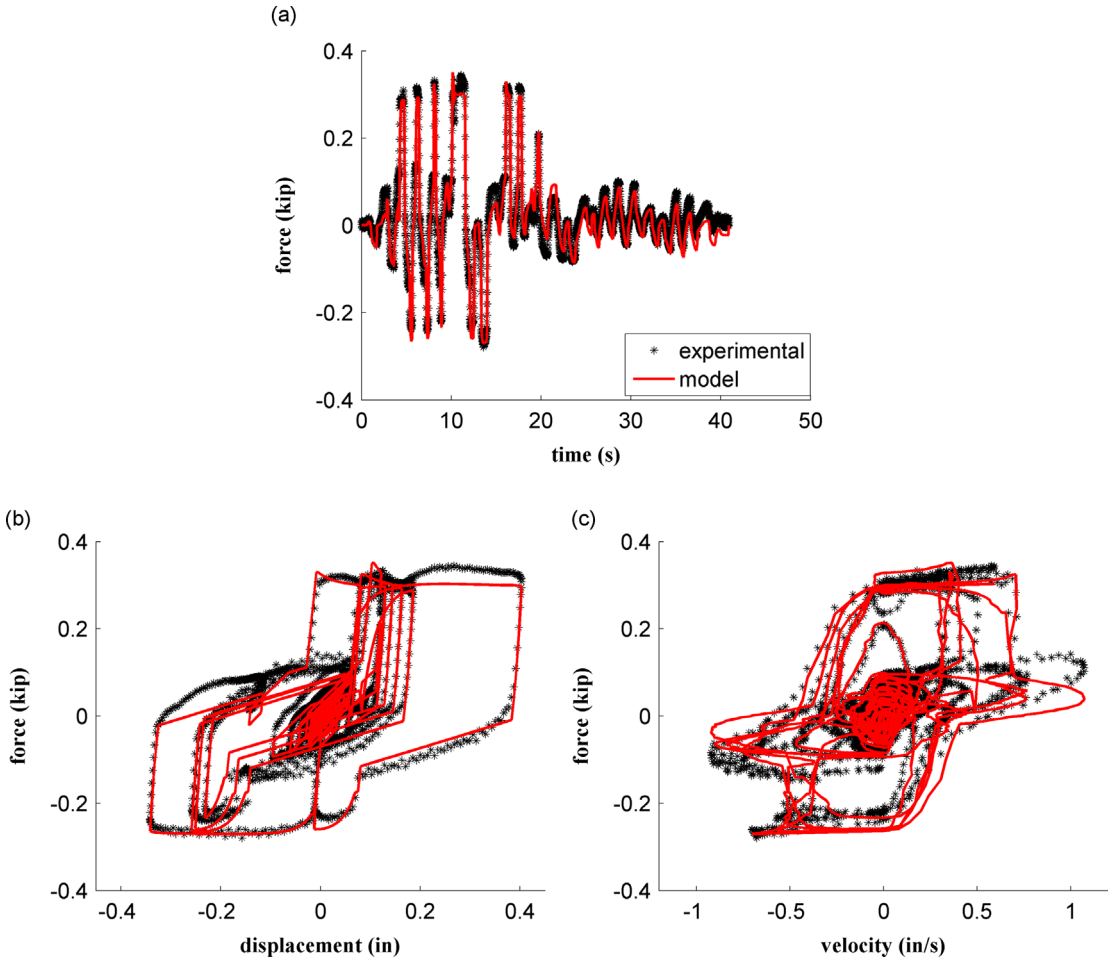

Fig. 14. Kobe earthquake at 500 psi: (a) time history of damper force; (b) force–displacement loop; (c) force–velocity loop.

Tables 2 and 3 list the values obtained experimentally (exp.) and from the optimized model for both low (2) and higher (3) excitation frequencies. The experimental value for σ_0 could not be obtained under 0 pressure due to the relatively high level of noise in the very small force output measurements. Its analytical value (model) was obtained by linear interpolation.

Fig. 7 are plots of the forces obtained from the laboratory experiments and the optimized model, under both 0.05 Hz and 0.5 Hz.

Table 4 summarizes the optimized values for the dynamic model. Note that the forward friction force coefficients differ from the backward friction force coefficients due to the asymmetry in the brake shoes.

Fitting results from the model are presented in Figs. 8–11. Experimental results obtained under 0.5 Hz show more noise with respect to results obtained at 0.05 Hz, likely due to chattering. This phenomenon will require further investigation. Results show a good fit between the experimental results and the model. There is a notable fitting discrepancy at low frequency under low pressure (500 psi and 800 psi), which indicate possible nonlinearities during Stage 2. Fig. 12 shows the combined force–displacement (Fig. 12(a)) and force–velocity (Fig. 12(b)) loops plotted using the model for a harmonic excitation of 1 in at 0.50 Hz.

5. Model validation: earthquake excitations

5.1. Methodology

The proposed dynamic model is verified over time-varying displacement and velocity inputs. Two earthquake excitations are selected due to their rich frequency content and varying amplitudes, representing an extreme input on a characterization perspective. Note that in applications, the MFD would be installed within a structural system and the structure would act as a low-pass filter, reducing the high frequency demand on the device. The first excitation is the 1979 Imperial Valley Earthquake

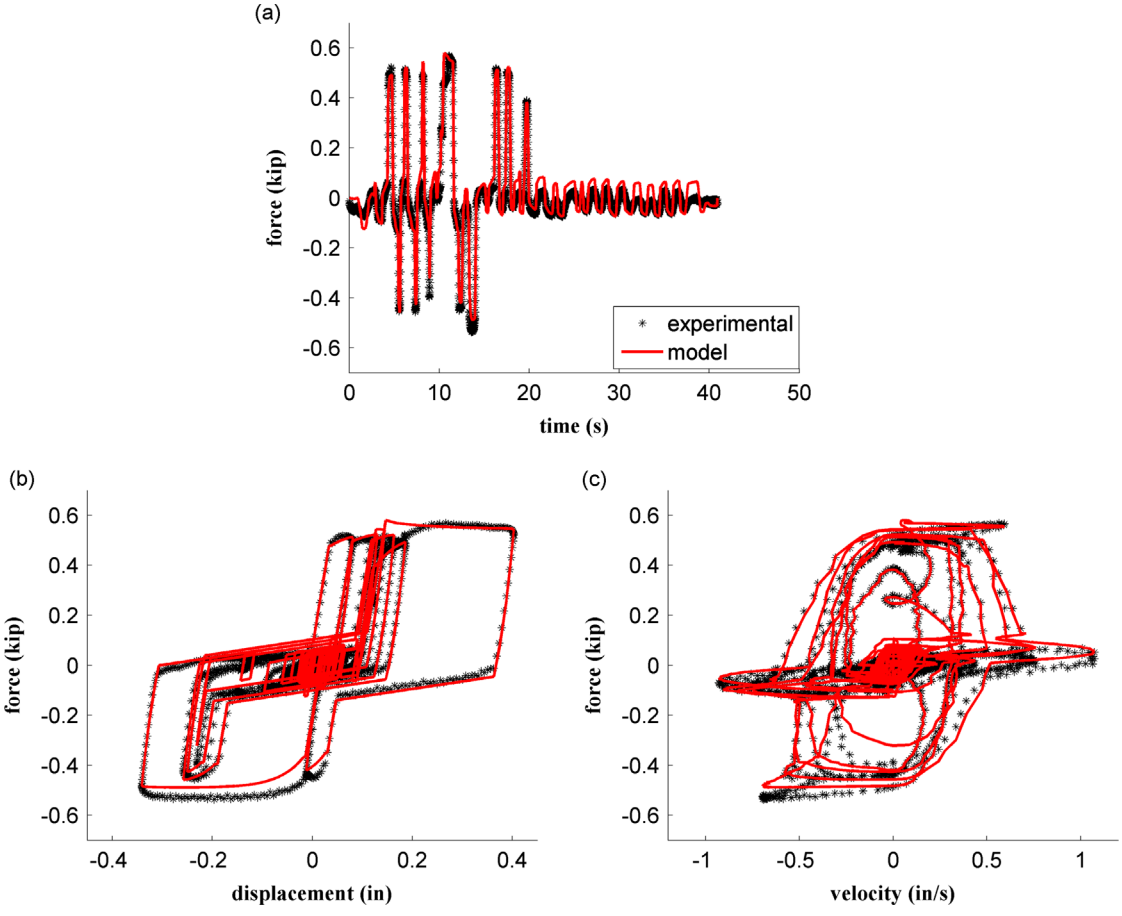

Fig. 15. Kobe earthquake at 1000 psi: (a) time history of damper force; (b) force–displacement loop; and (c) force–velocity loop.

record from the USGS Station 5155. The second excitation is the 1995 Kobe Earthquake record from the Kakogawa USGS Station CUE90. The acceleration time series of these records were obtained from the PEER ground motion record database (records P0174 and P1041) [34]. Ground displacements were computed by double integrating the ground acceleration, and scaled to a maximum displacement of 0.4 in to match the testing equipment's limitations at high frequencies. Acceleration and scaled displacement time histories are as shown in Fig. 13. Two different constant pressure values are used in the experiment: 500 psi, a value parameterized above, and 1000 psi, a value not parameterized previously.

5.2. Results and discussion

Figs. 14–17 show the time history, force–displacement, and force–velocity plots for each seismic excitation, in which the experimental data are compared with values from the proposed model. There is a good match of the theoretical model with the experimental data under both levels of pressure. However, there is a larger discrepancy in the fitting when the friction force is low and the displacements are small. This lower performance is also more evident under low pressure (500 psi). The possible nonlinearity in Stage 2 of the model found under the harmonic excitations is also apparent in this set of experimental results. In particular, Fig. 15(a) shows an overshoot of the estimated force after approximately 20 s. This overshoot is due to the linear approximation of the damping force when the shoes are slipping (stage 2), further evidenced in Fig. 15(b) by the overestimation of the experimental data for low forces (between approximately −0.15 and 0.15 kip).

From these results, the characterization of Stage 2 requires further investigation. However, dynamic Stages 2 and 3 that are unique to a duo-servo drum brake due to the planned sticking of braking shoes result in a suboptimal performance of the semi-active damping system. By eliminating the gap between the shoes and the anchor pin, the friction dynamics would cover a larger region in the force–displacement loop, thus enabling higher energy dissipation. A second generation of the

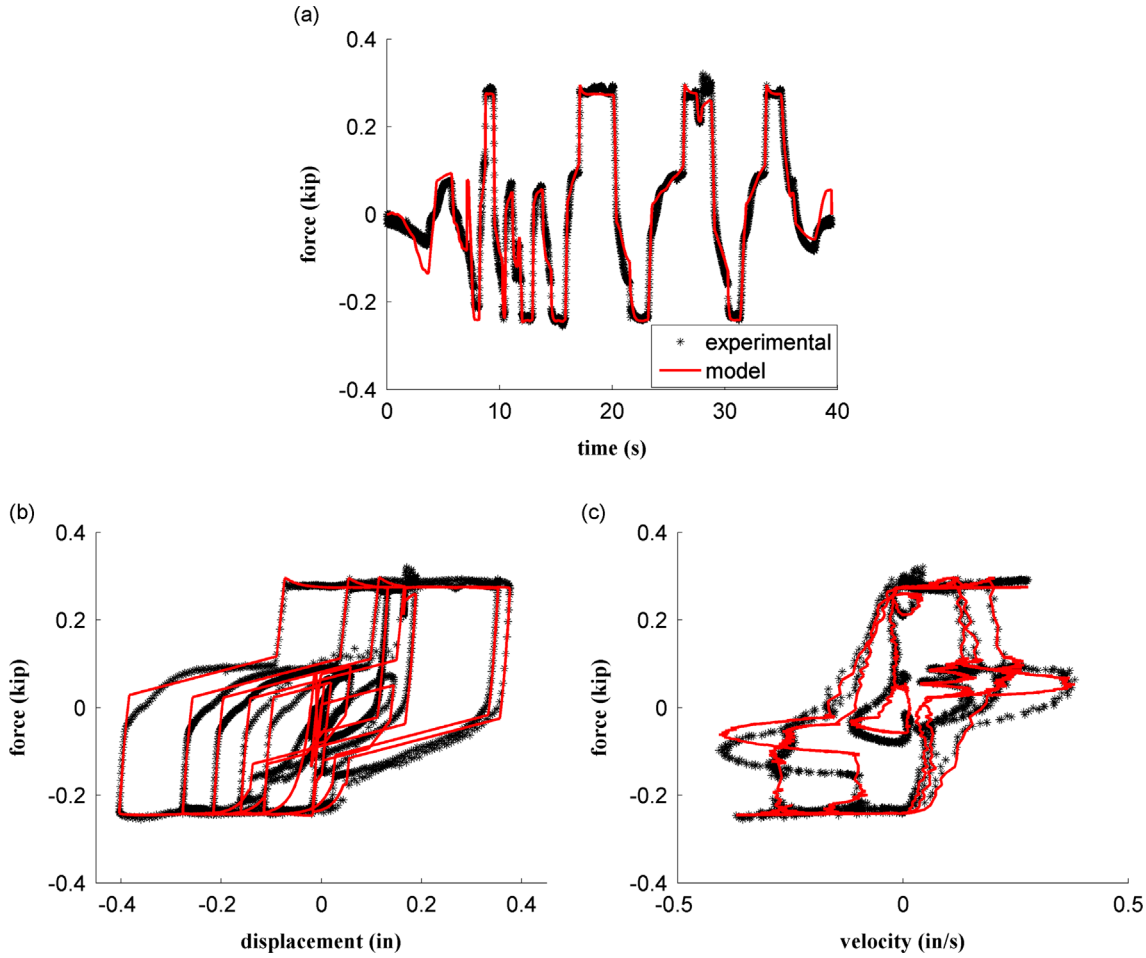

Fig. 16. Imperial Valley earthquake at 500 psi: (a) time history of damper force; (b) force–displacement loop; (c) force–velocity loop.

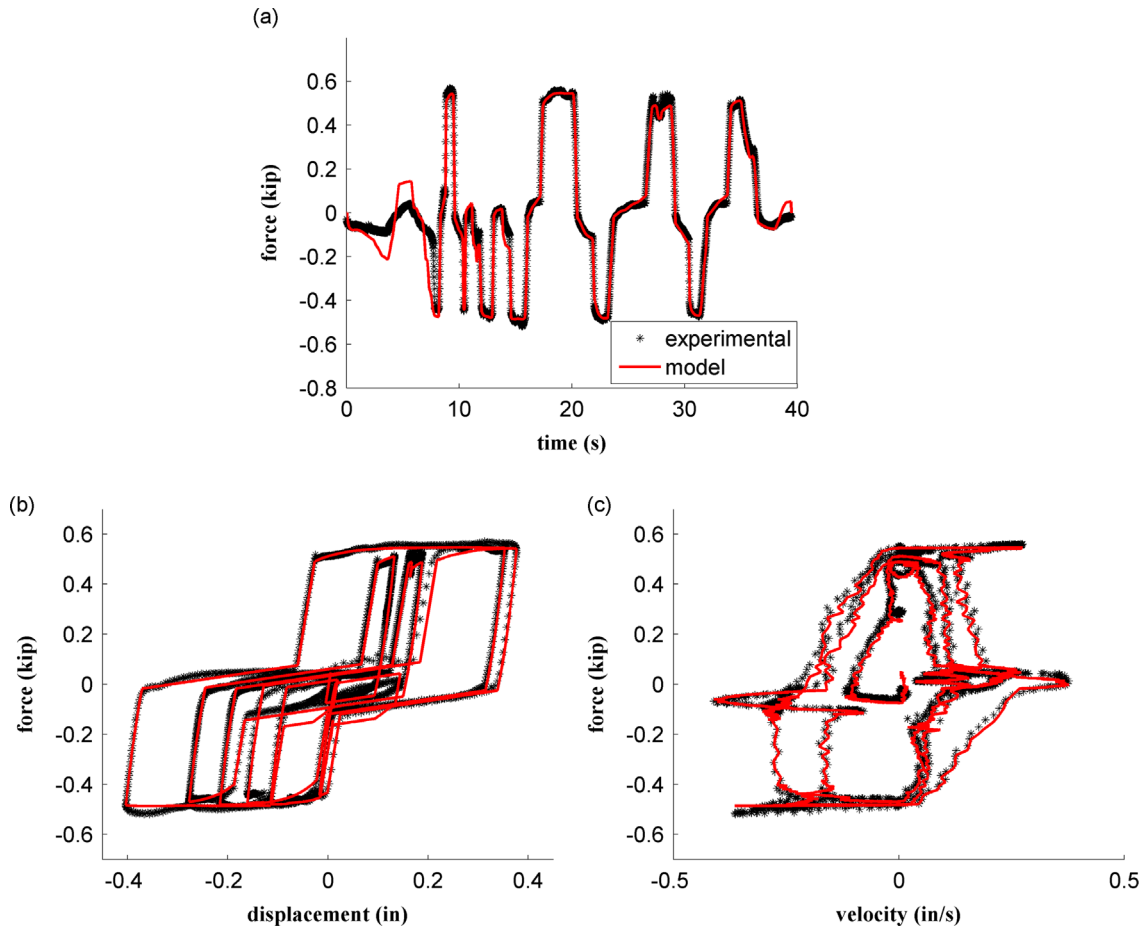

Fig. 17. Imperial Valley earthquake at 500 psi: (a) time history of damper force; (b) force–displacement loop; (c) force–velocity loop.

MFD is currently being designed to reduce (or eliminate) the dynamics provoked by the presence of Stages 2 and 3. Nevertheless, the utilization of an off-the-shelf due-servo drum brake is convenient due to its readily availability.

6. Summary and conclusions

We have characterized the dynamic behavior of a novel semi-active friction device designed for structural control. A particular feature of the due-servo drum brake is the discontinuity of the friction dynamics due to the gap between the anchor pin and braking shoes. A 3-stage dynamic model was proposed to characterize this dynamics. A LuGre friction model was used to model the friction zone (Stage 1), and two pure stiffness regions to characterize the dynamics of the MFD once the rotation is reversed and the braking shoes are sticking to the drum (Stage 2) and the rapid build up of forces once the shoes are held by the anchor pin (Stage 3). A small-scale prototype was fabricated and the parameters of the dynamic model identified by subjecting the device to different harmonic excitations under various pressure inputs. The model was later validated using two different earthquake excitations under two pressure inputs.

Results show that the model was capable of tracking the device's response, despite a lower fitting performance under low pressure and small force output, as it was found for the harmonic tests during the model identification phase. A possible nonlinearity in Stage 2 of the dynamic model is responsible for most of this lower performance. Future investigation will include enhanced modeling of Stage 2's dynamics by using a nonlinear stiffness element to improve on model fitting, and a second-generation design to reduce the dynamics provoked by the gap between the anchor pin and the braking shoes (Stages 2 and 3) to improve energy dissipation.

The validated model in this research advances the understanding of the dynamic behavior of an automotive braking system used for structural control applications. Integrated in the MFD design, such technology provides a mechanically robust alternative to semi-active control of civil structures. The proposed model can be used to enhance design of structures equipped with MFD, and to develop effective control algorithms.

Acknowledgements

This material is based upon work supported by the National Science Foundation under Grant no. 1300960. Their support is gratefully acknowledged. Any opinions, findings, and conclusions or recommendations expressed in this material are those of the author(s) and do not necessarily reflect the views of the National Science Foundation.

References

[1] J.J. Connor, S. Laflamme, *Structural Motion Engineering*, Springer, New York, 2014. ISBN: 3319062808.
[2] M. Symans, F. Charney, A. Whittaker, M. Constantinou, C. Kircher, M. Johnson, R. McNamara, Energy dissipation systems for seismic applications: current practice and recent developments, *Journal of Structural Engineering* 134 (1) (2008) 3–21.
[3] I.H. Mualla, B. Belev, Performance of steel frames with a new friction damper device under earthquake excitation, *Engineering Structures* 24 (3) (2002) 365–371.
[4] A.S. Pall, C. Marsh, P. Fazio, Friction joints for seismic control of large panel structures, *Journal Prestressed Concrete Institute* 25 (6) (1980) 38–61.
[5] A.S. Pall, C. Marsh, Response of friction damped braced frames, *Journal of Structural Engineering* 108 (9) (1982) 1313–1323.
[6] A. Filiatrault, S. Cherry, Performance evaluation of friction damped braced steel frames under simulated earthquake loads, *Earthquake Spectra* 3 (1) (1987) 57–78.
[7] T. FitzGerald, T. Anagnos, M. Goodson, T. Zsutty, Slotted bolted connections in aseismic design for concentrically braced connections, *Earthquake Spectra* 5 (2) (1989) 383–391.
[8] C.E. Grigorian, T.-S. Yang, E.P. Popov, Slotted bolted connection energy dissipators, *Earthquake Spectra* 9 (3) (1993) 491–504.
[9] B. Morgen, Y. Kurama, A friction damper for post-tensioned precast concrete beam-to-column joints, *Precast/Prestressed Concrete Institute Journal* 49 (4) (2004) 112–133.
[10] Y.-C. Lin, R. Sause, J. Ricles, Seismic performance of a large-scale steel self-centering moment-resisting frame: *Mce hybrid simulations and quasi-static pushover tests*, *Journal of Structural Engineering* 139 (7) (2012) 1227–1236.
[11] V. Panchal, R. Jangid, Variable friction pendulum system for near-fault ground motions, *Structural Control and Health Monitoring* 15 (4) (2008) 568–584.
[12] M. Mirtaheri, A.P. Zandi, S.S. Samadi, H.R. Samani, Numerical and experimental study of hysteretic behavior of cylindrical friction dampers, *Engineering Structures* 33 (12) (2011) 3647–3656.
[13] S. Kannan, H.M. Uras, H.M. Aktan, Active control of building seismic response by energy dissipation, *Earthquake Engineering and Structural Dynamics* 24 (5) (1995) 747–759.
[14] T. Vesselenyi, S. Dzitac, I. Dzitac, M.-J. Manolescu, Fuzzy and neural controllers for a pneumatic actuator, *International Journal of Computers Communications and Control* 2 (4) (2007) 375–387.
[15] A. Mehmood, S. Laghrouche, M. el Bagdouri, Modeling identification and simulation of pneumatic actuator for vgt system, *Sensors and Actuators A: Physical* 165 (2) (2011) 367–378.
[16] J.N. Yang, A.K. Agrawal, Semi-active hybrid control systems for nonlinear buildings against near-field earthquakes, *Engineering Structures* 24 (3) (2002) 271–280.
[17] M. Lorenz, B. Heimann, V. Härtel, A novel engine mount with semi-active dry friction damping, *Shock and Vibration* 13 (4) (2006) 559–571.
[18] S. Narasimhan, S. Nagarajaiah, Smart base isolated buildings with variable friction systems: *H controller and saivf device*, *Earthquake Engineering and Structural Dynamics* 35 (8) (2006) 921–942.
[19] Y. Kawamoto, Y. Suda, H. Inoue, T. Kondo, Electro-mechanical suspension system considering energy consumption and vehicle manoeuvre, *Vehicle System Dynamics* 46 (S1) (2008) 1053–1063.
[20] C. Chen, G. Chen, Shake table tests of a quarter-scale three-storey building model with piezoelectric friction dampers, *Structural Control and Health Monitoring* 11 (4) (2004) 239–257.
[21] L.-Y. Lu, G.-L. Lin, A theoretical study on piezoelectric smart isolation system for seismic protection of equipment in near-fault areas, *Journal of Intelligent Material Systems and Structures* 20 (2) (2009) 217–232.
[22] O. Durmaz, W.W. Clark, D.S. Bennett, J.S. Paine, M.N. Samuelson, Experimental and analytical studies of a novel semi-active piezoelectric coulomb damper, In: SPIE's 9th Annual International Symposium on Smart Structures and Materials, International Society for Optics and Photonics, 2002, pp. 258–273.
[23] Y. Xu, C. Ng, Seismic protection of a building complex using variable friction damper: experimental investigation, *Journal of Engineering Mechanics* 134 (8) (2008) 637–649.
[24] H. Dai, Z. Liu, W. Wang, Structural passive control on electromagnetic friction energy dissipation device, *Thin-Walled Structures* 58 (2012) 1–8.
[25] A.K. Agrawal, J.N. Yang, *Semiactive Control Strategies for Buildings Subject to Near Field Earthquakes* (2000) 359–370.
[26] S. Laflamme, D. Taylor, M. Abdellaoui Maane, J.J. Connor, Modified friction device for control of large-scale systems, *Structural Control and Health Monitoring* 19 (4) (2012) 548–564.
[27] D.P. Taylor, Toggle brace dampers: a new concept for structural control, *Proceedings of the 2000 Structures Congress and Exposition on Advanced Technology in Structural Engineering*, 2000.
[28] C. Huang, R. McNamara, The efficiency of the motion amplification device with viscous damper, 8th National Conference for Earthquake Engineering, vol. 62, 2006.
[29] M.C. Constantinou, P. Tsopelas, W. Hammel, A.N. Sigaher, Toggle-brace-damper seismic energy dissipation systems, *Journal of Structural Engineering* 127 (2) (2001) 105–112.
[30] K.R.M. Mahmoud, Theoretical and Experimental Investigations on a New Adaptive Duo Servo Drum Brake with High and Constant Brake Shoe Factor, HNI, 2005.
[31] S. Laflamme, J. Slotine, J. Connor, Wavelet network for semi-active control, *Journal of Engineering Mechanics* 137 (7) (2011) 462–474.
[32] H. Olsson, K.J. Åström, C. Canudas de Wit, M. Gäfvert, P. Lischinsky, Friction models and friction compensation, *European Journal of Control* 4 (3) (1998) 176–195.
[33] R. Jiménez, L. Álvarez-Icaza, Lugre friction model for a magnetorheological damper, *Structural Control and Health Monitoring* 12 (1) (2005) 91–116.
[34] Peer. Pacific Earthquake Engineering Research Center, 2010, URL: ⟨http://peer.berkeley.edu/peer_ground_motion_database⟩.